Sperm-Associated Antigen–17 Gene Is Essential for Motile Cilia Function and Neonatal Survival

Maria Eugenia Teves[1], Zhibing Zhang[1,2], Richard M. Costanzo[3], Scott C. Henderson[4], Frank D. Corwin[5], Jamal Zweit[2,5], Gobalakrishnan Sundaresan[5], Mark Subler[6], Fadi N. Salloum[7], Bruce K. Rubin[3,8], and Jerome F. Strauss III[1,2]

[1]Department of Obstetrics and Gynecology, [2]Department of Biochemistry and Molecular Biology, [3]Department of Physiology and Biophysics, [4]Department of Anatomy and Neurobiology, [5]Department of Radiology, [6]Department of Human and Molecular Genetics, [7]Pauley Heart Center, Division of Cardiology, Department of Internal Medicine, and [8]Department of Pediatrics, Virginia Commonwealth University, Richmond, Virginia

Primary ciliary dyskinesia (PCD), resulting from defects in cilia assembly or motility, is caused by mutations in a number of genes encoding axonemal proteins. PCD phenotypes are variable, and include recurrent respiratory tract infections, bronchiectasis, hydrocephaly, situs inversus, and male infertility. We generated knockout mice for the sperm-associated antigen–17 (*Spag17*) gene, which encodes a central pair (CP) protein present in the axonemes of cells with "9 + 2" motile cilia or flagella. The targeting of *Spag17* resulted in a severe phenotype characterized by immotile nasal and tracheal cilia, reduced clearance of nasal mucus, profound respiratory distress associated with lung fluid accumulation and disruption of the alveolar epithelium, cerebral ventricular expansion consistent with emerging hydrocephalus, failure to suckle, and neonatal demise within 12 hours of birth. Ultrastructural analysis revealed the loss of one CP microtubule in approximately one quarter of tracheal cilia axonemes, an absence of a C1 microtubule projection, and other less frequent CP structural abnormalities. SPAG6 and SPAG16 (CP proteins that interact with SPAG17) were increased in tracheal tissue from SPAG17-deficient mice. We conclude that *Spag17* plays a critical role in the function and structure of motile cilia, and that neonatal lethality is likely explained by impaired airway mucociliary clearance.

Keywords: primary ciliary dyskinesia; axoneme; central pair; *Spag17*; cilia

Cilia are organelles that play key roles, including the determination of left–right asymmetry in the body; clearing mucus, particles, and fluid out of the airways; and facilitating the flow of cerebrospinal fluid (CSF) (1). Primary ciliary dyskinesia (PCD), which results from defects in the formation and function of cilia and flagella, is a relatively rare disorder affecting 1 in 16,000 individuals worldwide (2). The axoneme, the highly conserved cytoskeletal structure of motile cilia, has a "9 + 2" arrangement consisting of nine outer doublet microtubules surrounding a central microtubule pair. Motility is dependent upon proteins associated with the outer doublet microtubules, including dynein arms, radial spokes, and nexin links.

The sliding of the outer doublet microtubules is modulated by the central pair (CP) apparatus (2–4). The two microtubules in the CP are structurally and biochemically dimorphic, and by convention receive separate designations (e.g., C1 and C2). At least 10 different polypeptides are uniquely associated with the C1 microtubule, and seven are unique to the C2 microtubule (3–6). This biochemical and structural asymmetry is believed to have functional significance with respect to the cilia or flagellar beat and waveform (7).

The mammalian sperm-associated antigen–17 protein (SPAG17) is the orthologue of *Chlamydomonas reinhardtii* PF6 (8), a protein located on a projection from the C1 CP microtubule in green algae (9). The PF6 protein interacts with a number of other proteins, including calmodulin, and ultimately influences the radial spokes attached to the outer microtubule doublets (10). Consequently, PF6 is thought to be a proximal effector of CP action on the sliding activity of the outer doublets that control cilia or flagellar beat. *Chlamydomonas pf6* mutants demonstrate paralyzed flagella, and lack the CP 1a projection (9). The full-length murine SPAG17 protein is 250 kD, like its *Chlamydomonas* orthologue, and it is found in testes and tissues with motile cilia (8, 11). The present study sought to determine whether mammalian SPAG17 plays an essential role in mammalian motile cilia.

CLINICAL RELEVANCE

We believe that the data presented in this study are worthy of broad readership because they point out the very significant differences between model organisms (e.g., *Chlamydomonas*) that have provided the foundation for our understanding of ciliary/flagellar axoneme biology, and mammalian motile cilia function. Our data also provide a hierarchy for the functional roles of central apparatus proteins, based on the phenotypes of mutant mice. Our observations are of relevance to clinical disorders of ciliary dysfunction (e.g., primary ciliary dyskinesia).

MATERIALS AND METHODS

Mice

All animal procedures were performed in accordance with the National Research Council's Guide for the Care and Use of Laboratory Animals. Animals were killed in accordance with protocol AM10297 approved by the Virginia Commonwealth University Institutional Animal Care and Use Committee. Further details are provided in the online supplement.

Targeted Disruption of *Spag17*

To knock out the *Spag17* gene, embryonic stem (ES) cells with conditional potential were obtained from the Knock Out Mouse Project Repository (Davis, CA). The ES cells were used to generate chimeric mice. The chimeric males were crossed to C57BL/6J wild-type females, and the resultant heterozygous offspring were crossed to 129S4/SvJaeSor-Gt(ROSA)26Sor$^{tm1(FLP1)Dym}$/J mice to remove the Neo cassette. The *Spag17*$^{+/flox}$ mice were used for mating with *CMV-Cre* (B6.C-Tg(CMV-cre)

(*Received in original form September 18, 2012 and in final form January 16, 2013*)

This work was supported by National Institutes of Health grant HD-37416 (J.F.S.) and a Virginia Commonwealth University Presidential Research Incentive Program Award (Z.Z.). Microscopy was performed at the Department of Anatomy and the Neurobiology Microscopy Facility at Virginia Commonwealth University, supported in part with funding from National Institutes of Health–National Institute of Neurological Disorders and Stroke Center Core Grant P30 NS047463.

Correspondence and requests for reprints should be addressed to Jerome F. Strauss III, M.D., Ph.D., Department of Obstetrics and Gynecology, Virginia Commonwealth University, Sanger Hall, Dean's Office, 1101 East Marshall Street, Richmond, VA 23298-0565. E-mail: jfstrauss@vcu.edu

This article has an online supplement, which is accessible from this issue's table of contents at www.atsjournals.org

Am J Respir Cell Mol Biol Vol 48, Iss. 6, pp 765–772, Jun 2013

Originally Published in Press as DOI: 10.1165/rcmb.2012-0362OC on February 13, 2013
Internet address: www.atsjournals.org

1Cgn/J) mice to generate *Spag17*$^{+/-}$*;CMV-Cre* mice. Male and female *Spag17*$^{+/-}$*;CMV-Cre* mice were mated, resulting in the expecting Mendelian inheritance for *Spag17*$^{-/-}$*;CMV-Cre* mice. After these matings, the mice demonstrated a mixed background of C57BL/6J–129S4/SvJ. Further details are provided in the online supplement.

Southern Blotting

Genomic DNA was digested with the *Bgl*II enzyme and subjected to Southern blot analysis, using a probe for *Spag17* detection. Details are provided in the online supplement.

RT-PCR

RT-PCR was performed to amplify the *Spag17* message from several tissues, using a primer set specific for murine *Spag17*. Details are provided in the online supplement.

Western Blotting

Proteins were extracted from murine tracheal tissues and subjected to Western blot analysis, using antibodies against SPAG17, SPAG6, SPAG16, and primary ciliary dyskinesia protein 1 (Pcdp1). Details are provided in the online supplement.

Immunohistochemistry

Brain tissue samples from wild-type and mutant mice were fixed and prepared for SPAG17 immunohistochemistry detection. Details are provided in the online supplement.

Immunofluorescence

Tracheal tissues from wild-type and mutant mice were fixed and prepared for SPAG17 immunofluorescence detection. Details are provided in the online supplement.

Magnetic Resonance Imaging

Two-hour-old wild-type and knockout mice pups were evaluated under magnetic resonance imaging for a morphological comparison of their bodies. Magnetic resonance imaging was performed with Bruker-Biospin Biospec console and a 7-Tesla, 30-cm free bore magnet (Bruker Biospin Corporation, Billerica, MA). Further details are provided in the online supplement.

Electron Microscopy

Ependymal and tracheal tissues from wild-type and mutant mice were fixed and prepared for transmission electron microscopy, according to standard methods. Further details are provided in the online supplement.

Two-Dimensional Image Averaging

Trachea were dissected from the mice pups and placed directly into fixative, and prepared for transmission electron microscopy. Images were first processed in Adobe Photoshop (Adobe Systems Inc., San Jose, CA), and the average intensity projections were generated in ImageJ (http://http://rsb.info.nih.gov/ij/). Further details are provided in the online supplement.

Video Microscopy

Tracheal and nasal tissues were observed with differential interference contrast microscopy. Movies were recorded at 30 frames per second with a Sanyo Hi-Resolution camera (Sanyo Electric Co., Moriguchi City, Japan). Movies were edited using Pinnacle Studio HD software, version 14.0 (Pinnacle Systems, Inc., Mountain View, CA). Further details are provided in the online supplement.

Micro-Computed Tomography

Micro–computed tomography (micro-CT) was performed using an Inveon Micro-CT system (Siemens, Knoxville, TN). Image segmentation, analysis, and volume rendering were performed using Inveon Research Workplace, version 4.0 (Siemens). Further details are provided in the online supplement.

Echocardiography

Echocardiography was performed using the Vevo770 imaging system (Visual Sonics, Inc., Toronto, ON, Canada). Further details are provided in the online supplement.

RESULTS

The Phenotype of SPAG17-Deficient Mice

Mice deficient in SPAG17 were generated through breeding to CMV-Cre, which is expressed in all tissues (Figure 1). Nullizygous pups died within 12 hours of birth, whereas heterozygous mutants were viable and no different from their wild-type littermates. The genotyping of pups immediately after birth demonstrated that the mutant allele was transmitted in a pattern that was not significantly different from that anticipated for Mendelian inheritance (*see* Table E1 in the online supplement). Longitudinal observations demonstrated that during the first hours after birth, the homozygous pups were indistinguishable from their heterozygous and wild-type littermates (Figure 2A). However, within 6–8 hours after birth, the homozygous mutant mice developed severe respiratory distress, with labored breathing and cyanotic skin (Video E1, and Figure 2B). In addition, the homozygous mutant mice could not suckle, so they lacked "milk spots" in their stomachs (Figure 2B), consistent with abnormal feeding. Furthermore, as shown in Video E2, the homozygous mutant newborn pups displayed a limited capacity for movement and locomotion. All of the longitudinally observed nullizygous mice died within 12 hours of birth, whereas all heterozygous mutant and wild-type mice survived (Table E1).

To investigate the neonatal lethal phenotype further, magnetic resonance (MR) scanning studies on newborn pups were performed. The axial views from MR scans showed ventricular expansion in the brains of *Spag17*$^{-/-}$ mice, consistent with hydrocephalus (Figure 3A, *red*). In addition, lungs from null mice were full of fluid (Figure 3A, *green*). Examination of brains by histology revealed enlarged lateral ventricles, consistent with the MR scans (Figure 3B). Similarly, the histological examination of lung tissue suggested fluid accumulation, and revealed the disruption of alveolar epithelia (Figures 2C and 2F). Analyses of paranasal sinuses revealed that excessive mucus accumulated in the mutant animals (Figure 2D).

Micro-CT studies were performed in wild-type and knockout mice. Axial images from *Spag17*$^{-/-}$ mice with detectable labored breathing reveled a reduced presence of air in the lungs (Figure 2G). In addition, a three-dimensional reconstruction from micro-CT studies indicated less lung expansion in the mutant mice (Video E3).

Although the *Spag17* mutants developed a phenotype consistent with PCD, we did not find situs inversus in the *Spag17*$^{-/-}$ mice, which is in accordance with findings in other CP protein knockout murine models (11–14). Moreover, no cardiac structural defects were observed in nullizygous mice (Figure E1A in the online supplement). However, ultrasound studies showed a reduced heart rate in *Spag17*$^{-/-}$ cyanotic mice, consistent with severe respiratory distress (Figure E1B).

Because Spag17 knockout mice develop profound respiratory distress within a few hours of birth, we analyzed the lung histology of wild-type and nullizygous pups before they exhibited detectable labored breathing and cyanosis. As shown in Figure 2I, the lung histology from *Spag17*$^{-/-}$ mice appeared normal. Neither fluid accumulation nor alveolar disruption was observed.

Cilia Motility Defects in SPAG17-Deficient Mice

To determine whether the motility of cilia was affected in the knockout mice, we examined the ciliary movement in tracheal

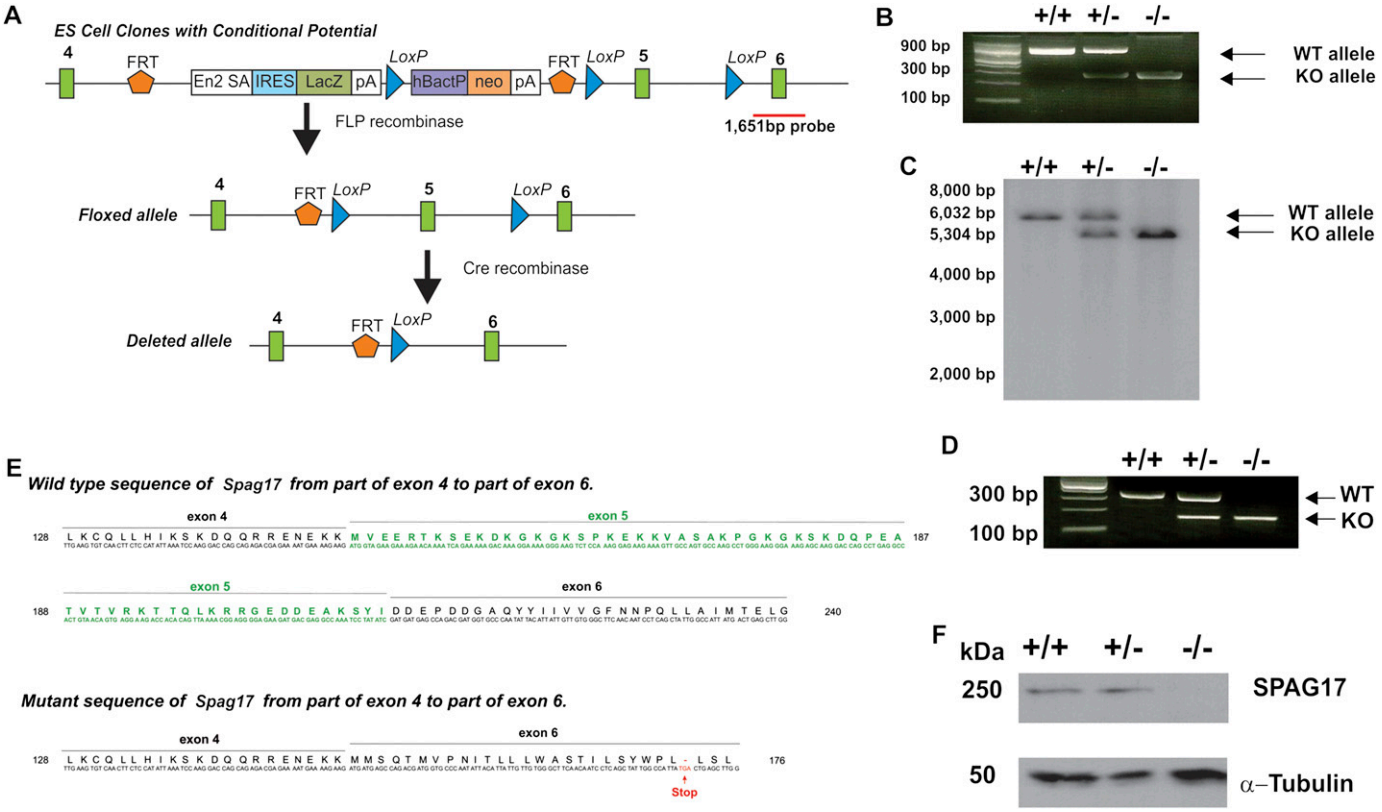

Figure 1. Targeted disruption of the murine sperm-associated antigen–17 (*Spag17*) gene. The murine *Spag17* gene is located in chromosome 3 and contains 49 exons. An embryonic stem (ES) cell line (C57BL/6N background) in which exon 5 was floxed for conditional targeting (Clone EPD0234_6_G08) was obtained from the Knock Out Mouse Project Repository (Davis, CA). The ES cell clone was used to generate chimeric mice. Chimeric males were crossed to C57BL/6J wild-type females, and the resulting heterozygous offspring were crossed to 129S4/SvJaeSor-Gt(ROSA)26Sor$^{tm1(FLP1)Dym}$/J mice to remove the Neo cassette. *Spag17*$^{+/flox}$ mice were mated to *CMV-Cre* mice to generate *Spag17*$^{+/-}$;*CMV-Cre* mice. Male and female *Spag17*$^{+/-}$;*CMV-Cre* mice were mated to create the *Spag17*$^{-/-}$;*CMV-Cre* mice. (*A*) Schematic representation of the strategy used to disrupt *Spag17* gene. *Red line* shows the probe location used for Southern blotting. ES, embryonic stem; FRT, flippase recognition target; LoxP, Lox-flanked cassette; En2 SA, splicing acceptor region of the En2 gene; IRES, internal ribosome-entry site; LacZ, beta-galactosidase gene; pA, polyadenylation site; neo, neomycin resistance gene; hBactP, human beta-actin promoter. (*B*) Genotypic analysis applied primers flanking upstream from the first FRT site, and downstream from the third LoxP site. (*C*) Southern blot analysis used *Bgl*II-digested genomic DNA from wild-type, heterozygous, and homozygous mutant mice. (*D*) Representative RT-PCR used primers in exon 4 (forward) and 6 (reverse). (*E*) Sequence result for wild-type (WT) and knockout (KO) alleles from RT-PCR products, after thymine-adenine (TA) cloning. (*F*) Immunoblotting of murine tracheal tissue extracts with rabbit anti-SGAP17 antibody, which reacts with the murine SPAG17 C-terminus. The blot shown is representative of three independent experiments, and tissues from three different mice in each genotype are shown.

and nasal tissue, using video-microscopy. Most of the cilia from *Spag17*$^{-/-}$ mice were immotile (Video E4), and only a few cells displayed cilia with an uncoordinated beat (Video E5). The density of cilia in the nullizygous mice appeared to be similar to that in heterozygous mutant and wild-type mice in these videos. In contrast, the cilia of *Spag17*$^{+/-}$ and *Spag17*$^{+/+}$ mice showed normal and coordinated motility (Video E6). Immotile cilia were also observed in nasal respiratory epithelia from mutant mice, whereas normal cilia motility was evident in wild-type mice (Video E7). The tracheas were removed from wild-type and knockout mice and were kept in PBS, with a drop of murine blood cells injected into the tracheal tube. The transit of these blood cells was evaluated using video microscopy. Video E8 shows the movement of blood cells driven by the coordinated ciliary beat in wild-type mice. However, no directed flow was detected, and blood cells were not moved, in the mutant murine tracheal preparations (Video E9).

Axoneme Structural Defects in SPAG17-Deficient Mice

The transmission electron microscopy of cilia from tracheal epithelia demonstrated that 23.7% of the axonemes from homozygous mutant mice were missing one CP microtubule, whereas none of the cilia in tracheas from either heterozygous or wild-type mice demonstrated these defects (Table E2A and Figures 4B and 4D). To analyze the CP projections, two-dimensional image-averaging techniques were performed in the axonemes where the two CPs were present. As shown in Figure 5, the axoneme of *Spag17*$^{-/-}$ mice appears to lack a C1 projection (i.e., the putative orthologue of the C1a projection of *Chlamydomonas*). Moreover, the distance between the two CP microtubules was significantly greater in the homozygous mutant than in the wild-type mice, and the density of the bridges between the two CP microtubules was reduced (Table E2B). These abnormalities were not observed in airway cilia from heterozygous mutant or wild-type mice. We also observed that some *Spag17* nullizygous mice possessed axonemes with a third central microtubule ("9 + 3"), a phenotype that has not been previously reported in *Chlamydomonas* or the mouse (Figure E2). These findings suggest that SPAG17 plays both a structural and functional role in the ciliary axoneme.

CP Protein Expression in SPAG17-Deficient Mice

Western blotting revealed that the 250-kD SPAG17 protein was absent from the trachea (Figure 1F), and immunofluorescence (Figure E3A) and immunocytochemistry studies (Figure E3B)

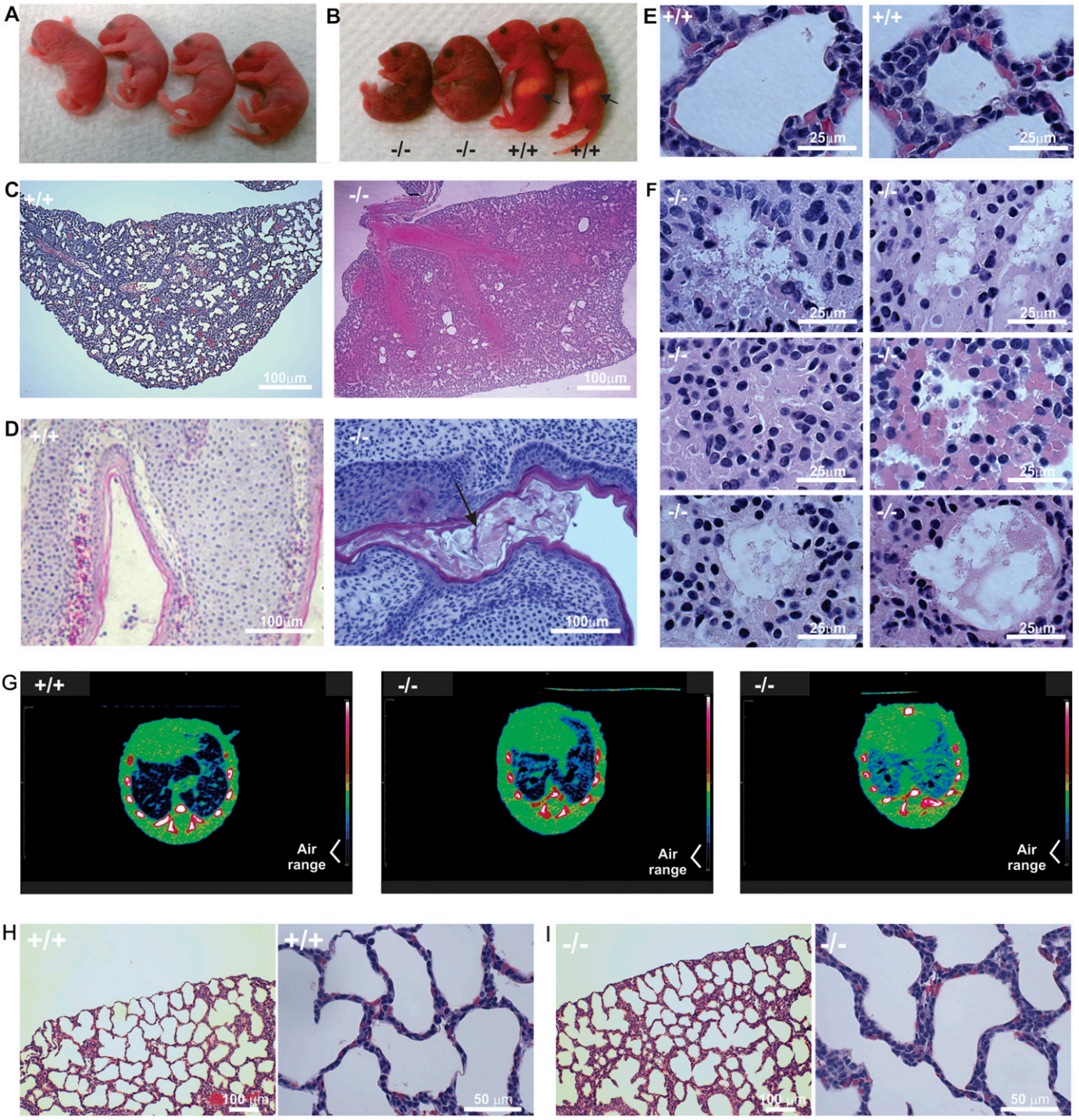

Figure 2. Deletion of *Spag17* gene expression results in hydrocephalus and pulmonary and nasal mucus and fluid congestion. (*A*) Four littermates with indistinguishable phenotypes within one hour of birth. (*B*) Pups from the same litter show abnormal phenotypes a few hours after birth. Pups were genotyped by PCR after photograph was taken. *Arrows* show the presence of milk spot in wild-type mice. (*C*) Histologic sections from *Spag17*$^{+/+}$ and *Spag17*$^{-/-}$ mice. Lung tissue from *Spag17*$^{-/-}$ mouse appears to be full of fluid. (*D*) Paranasal cavities with the presence of mucus (*arrow*) in a nullizygous mouse. (E) Higher magnification images from *Spag17*$^{+/+}$ mouse show normal lung-tissue structure. (*F*) Higher magnification images from *Spag17*$^{-/-}$ mouse show fluid infiltration, edema, and the disruption of alveolar epithelia. (*G*) Representative micro–computed tomography axial images from one *Spag17*$^{+/+}$ mouse and two *Spag17*$^{-/-}$ mice with detectable labored breathing revealed a reduced presence of air in the lungs. (*H*) Lung histology from *Spag17*$^{+/+}$ mouse. (*I*) Lung histology immediately after birth, before respiratory distress was evident.

confirmed the absence of protein in tracheal epithelial cells and brain ependymal cells from *Spag17*$^{-/-}$ mice.

We also evaluated the expression of SPAG6 (the murine orthologue of a *Chlamydomonas* protein, PF16, associated with the C1 microtubule), SPAG16 (the murine orthologue of a *Chlamydomonas* protein, PF20, that is located in the bridge between the C1 and C2 microtubules), and Pcdp1 (the murine orthologue of a *Chlamydomonas* protein associated with the C1 microtubule) by Western blot analysis in tracheal tissue from *Spag17*$^{+/+}$, *Spag17*$^{+/-}$, and *Spag17*$^{-/-}$ mice. The SPAG17 null mice demonstrated significantly

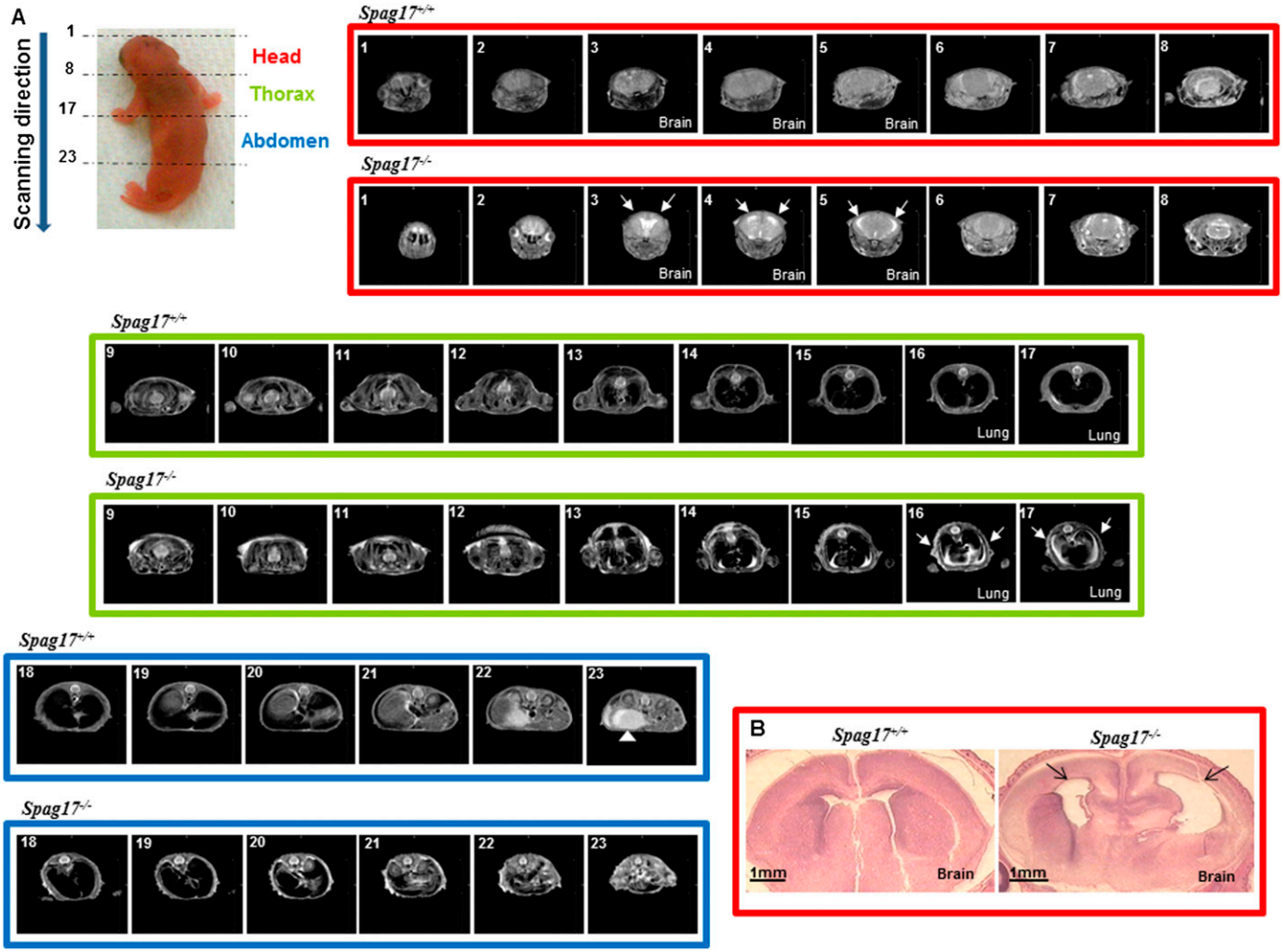

Figure 3. Mutation of the *Spag17* gene results in hydrocephalus and lung fluid accumulation. (*A*) Two-hour-old wild-type and knockout mice were evaluated using magnetic resonance imaging for a morphological comparison of their bodies. *Left*: The direction of the scanning images for each section. *Right*: Axial views from the head, thoracic, and abdominal sections. *Arrows* in the head sections point to ventricular expansion in the brain of a *Spag17*$^{-/-}$ mouse, consistent with hydrocephalus. *Arrows* in the thoracic section show the fluid-filled lung from a null mouse. *Arrowhead* in the abdominal section from a wild-type mouse identifies the presence of a milk spot, which is absent in the *Spag17*$^{-/-}$ mouse. (*B*) Representative axial views from brain tissues stained with hematoxylin and eosin. *Arrows* indicate the expansion of ventricles.

increased levels of SPAG6 and SPAG16L proteins compared with wild-type mice (Figures E4A and E4B). The levels of these proteins were also increased in heterozygous mutants, although the increase was not statistically significant. However, Pcdp1 was significantly reduced in *Spag17*$^{-/-}$ mice compared with wild-type and heterozygous mutants (Figure E4C). These observations could reflect defects in the assembly of CP components that result in accumulation (SPAG6 and SPAG16L) or instability (Pcdp1) proteins in the absence of SPAG17.

DISCUSSION

PCD, characterized by immotile cilia in various tissues and immotile sperm, is a dramatic example of axoneme dysfunction. It is a heterogeneous genetic disorder that affects 1 in 16,000 individuals. Mutations in 12 genes are associated with PCD, mainly those encoding the dynein arms (15), but an estimated two thirds of cases have yet to be assigned a molecular defect (16). The phenotypes of individuals with PCD are variable, but a clear understanding of how specific mutations cause different phenotypes is lacking (15). The discovery that murine mutations in the central apparatus protein genes, *Spag6* and *Spag16*, cause male infertility (and hydrocephalus in the case of *Spag6*), but not situs inversus (12, 17), supports the notion that lateralization defects in PCD are attributable to the dysfunction of "9 + 0" cilia, which fulfill different roles compared with "9 + 2" cilia (18). However, other phenotypic differences among PCD subjects remain to be explained. Human mutations or putative deleterious genetic variants have been identified in genes encoding central apparatus proteins, including the recent discovery of human *Hydin* mutations (19). Some of these variants or mutations might also modify the disease phenotype in PCD or other diseases involving pulmonary dysfunction, such as cystic fibrosis (16, 17).

The phenotype in SPAG17-deficient mice of rapid neonatal demise, evidently from respiratory failure, is consistent with airway ciliary dysfunction. Mice deficient in FOXJ1 (C57BL/6J background), a transcription factor that controls ciliogenesis, lack cilia, and most nullizygous offspring die immediately after birth, although a small number (8%) survive the neonatal period (20). Moreover, mice with other targeted mutations that create a PCD phenotype, including *Mdnah5*$^{-/-}$ (C57BL/6 × CBA/J

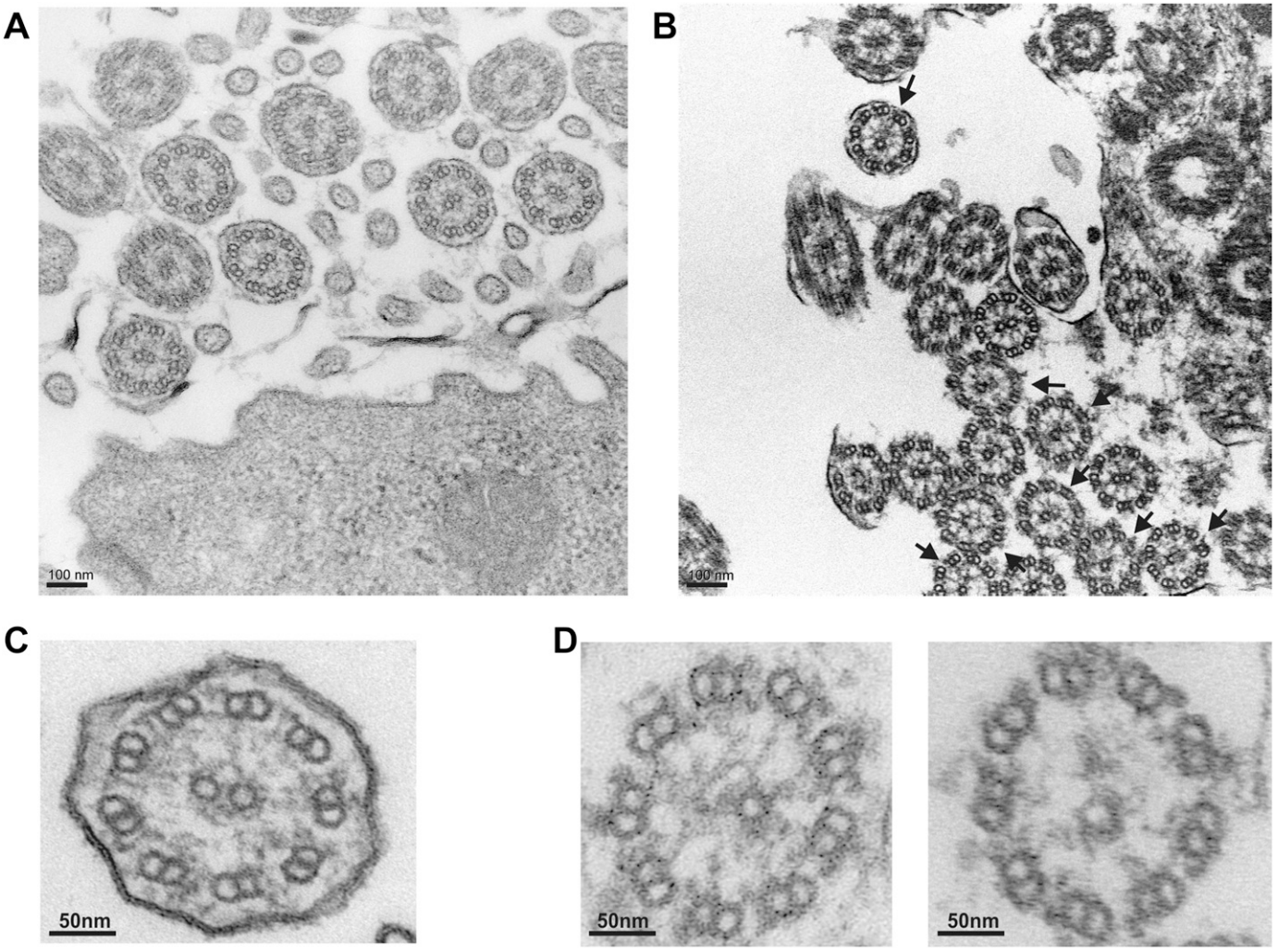

Figure 4. Targeted mutation of the *Spag17* gene causes a central pair (CP) defect. (*A*) Transmission electron micrograph from a *Spag17*$^{+/+}$ mouse depicts a "9 + 2" microtubule arrangement. (*B*) Transmission electron micrograph from a *Spag17*$^{-/-}$ mouse depicts axonemes lacking a microtubule in the CP (*arrows*). (*C*) High-magnification electron micrograph from a *Spag17*$^{+/+}$ mouse depicts a "9 + 2" microtubule arrangement. (*D*) High-magnification electron micrographs from a *Spag17*$^{-/-}$ mouse depict axonemes lacking a microtubule in the central apparatus.

background) and *Dnah11*$^{-/-}$ (C3H/HeH background) mutants, have immotile cilia, but survive the neonatal period (21, 22). The fact that SPAG17-deficient mice (C57BL/6J–129S4/SvJ mixed background), which possess cilia with no or impaired motility, all died during the neonatal period may be related to differences in genetic background, which is known to affect the phenotypes of mice with mutations altering cilia function, or may be related to mutation-unique environmental interactions (e.g., with housing conditions). The abnormality in mucociliary clearance of SPAG17 knockout mice, exemplified by the accumulation of mucus in the paranasal sinuses and fluid in the lungs, may have contributed to the respiratory distress of this obligate nasal-breathing species. The facts that the lungs of SPAG17-deficient mice were histologically normal at birth, and that the pups were indistinguishable from their heterozygous and wild-type littermates immediately after delivery, suggest that the respiratory distress was a result of postnatal complications.

We found that cilia in *Spag17*$^{-/-}$ tracheas failed to clear particles effectively, and the lungs showed fluid accumulation and a disruption of alveolar structure several hours later, which may be a consequence of hypoxic damage. Acute hypoxia increases pulmonary artery pressure, resulting in epithelial malfunction, edema, and lung inflammation (23), leading to respiratory distress. Fluid build-up in the lungs results in death from asphyxia, as suggested by micro-CT observations. The cardiac function abnormality we observed (bradycardia) is consistent with a hypoxic state. Because respiratory failure is usually associated with the low survival of newborn mice (death within 12 hours of birth) (24), our observations suggest that *Spag17* knockout neonatal death is attributable to respiratory failure.

Feeding problems are probably also related to respiratory distress and ciliary dysfunction, and may have contributed further to the early neonatal deaths (24). The function of nasal cilia may have impaired olfaction, required for pups to seek their mothers. The inability to feed will result in neonatal death, and nonfeeding pups usually die within a window of 12–24 hours after birth (24).

Although the neonatal SPAG17-deficient mice displayed evidence for evolving hydrocephalus, hydrocephalus *per se* was not likely the proximate cause of neonatal death. Cilia on ependymal cells facilitate the flow of CSF in the brain, and the congenital hydrocephalus observed in the MR images and histological preparations likely reflected defects in CSF circulation. The development of hydrocephalus is influenced by murine strain, and

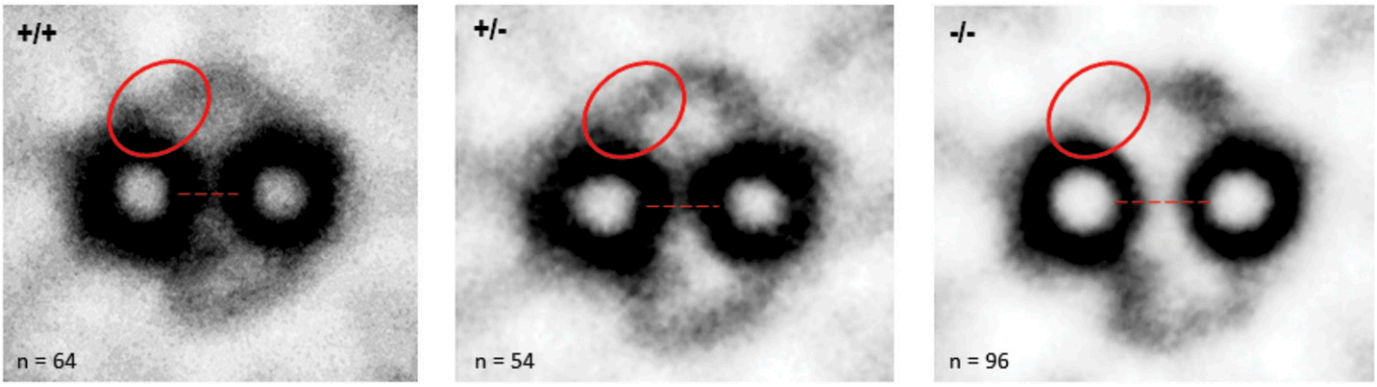

Figure 5. *Spag17* mutant mice demonstrate CP defects. Two-dimensional image-averaging techniques show a reduced bridge density and greater separation between the two CP microtubules (*dashed line*), and the absence of a C1 projection (*ovals*), probably the orthologue of the C1a projection of *Chlamydomonas*, in the knockout mice.

C57BL/6 mice more commonly develop hydrocephalus than do 129/Sv or mixed background mice (such as the *Spag17* knockout we studied). Although most of the knockout mice that developed hydrocephalus died, the ventricular dilatation was modest, and mice with more severe degrees of hydrocephalus (such as the mixed background SPAG6-deficient mice we previously created) survive for a week or two after birth (12).

The axoneme CP is involved in the control of ciliary and flagellar waveforms (2). Although the basic axonemal structure is highly conserved across species, cilia and flagella perform specialized functions unique to the tissue or cell in which they are present. For example, *Chlamydomonas* flagella can beat with two different waveforms and with high frequency, whereas respiratory mammalian cilia beat with a single waveform and much lower frequency. Recently, O'Toole and colleagues (25) demonstrated that most of the projections associated with each CP microtubule in *Chlamydomonas* appear to be conserved in human axonemes, although some differences are evident. For example, the C1a projection of *Chlamydomonas* appears to be more prominent compared with the human C1a projection, and an additional density adjacent to the C1c projection is present in humans. These findings suggest that functional differences may be reflected in small variations of structural organization (25).

The structural phenotype of axonemes in *Spag17* mutant mice is distinctive, showing similarities as well as differences in terms of the phenotype of *Chlamydomonas* axonemes lacking PF6, the protein orthologue of SPAG17. PF6-deficient *Chlamydomonas* lack the 1a projection off the C1 microtubule (5, 9, 26). We found that SPAG17-deficient mice were also missing a C1 projection, probably the orthologue of the *Chlamydomonas* C1a projection. In addition, approximately 25% of the tracheal ciliary axonemes were missing one CP microtubule, which is a structural phenotype similar to that in the *Chlamydomonas pf16* mutation, which is the orthologue of *Spag6*. These defects were not evident in the tracheal cilia of wild-type or heterozygous pups.

The loss of one CP microtubule has also been reported in humans with mutations in genes encoding radial spoke head proteins (27, 28). The similarity of structural abnormalities in the CP of the radial spoke head and *Spag17* mutants suggests that the nexus between the CP and the radial spokes is critical for stabilizing the axoneme.

SPAG6, the orthologue of *Chlamydomonas* PF16, is a protein associated with the C1 microtubule. Mice deficient in *Spag6* develop hydrocephalus, and 50% of these mice die within 8 weeks of birth. Surviving males are infertile because of impaired sperm motility (12). The axonemes of epididymal sperm tails exhibit ultrastructural abnormalities, including loss of the CP, but the axonemes of cilia in lung or ependymal cells appear to be normal.

SPAG16 is another CP protein, located in the bridge between the C1 and C2 microtubules. It is the orthologue of *Chlamydomonas* PF20. The *Spag16* gene encodes two major transcripts (*Spag16L* and *Spag16S*). Mice lacking SPAG16L are generally healthy, and the major phenotype involves male infertility because of a severe sperm motility defect (17, 29). The cilia of tracheal epithelia are motile in the absence of SPAG16L (Video E10). No gross abnormalities were observed in transmission electron micrographs of tracheal cilia in *Spag16*-deficient mice (17). The *Chlamydomonas pf20* mutant exhibits the most significant ultrastructural defects, lacking the entire CP. Thus, a totally different genotype–phenotype relationship exists among mutations in the CP genes of *Chlamydomonas* and mice, with a hierarchy in axoneme structural defects and functional deficits of *pf20* > *pf16* > *pf6* (most severe to least severe) and *Spag17* > *Spag6* > *Spag16* in mice.

Our previous studies suggested that SPAG17, SPAG6, and SPAG16L form an interactome (8, 11). In a previous Western blot analysis of testes and male germ cells, we found that when SPAG6 was absent (*Spag6* nulizygous mice), SPAG16L was also markedly reduced or missing, as was a germ-cell isoform of SPAG17 (8). In contrast, an increase in both SPAG6 and SPAG16 protein was evident in the tracheas of SPAG17-deficient mice. Although the molecular explanation for these observations remains unknown, it could reflect the instability of CP proteins in the absence of SPAG6, or the inability to assemble certain CP components into CP structures in the absence of SPAG17. It may also account for the reduced density of inter-CP microtubule bridges (SPAG16), and may contribute to the absence of the C1 microtubule projection in SPAG17-deficient mice. Interestingly, another putative C1-associated CP protein, Pcdp1, which is not known to be part of the aforementioned interactome, was reduced. Further studies are needed to elucidate the mechanisms underlying these changes in protein content.

The *Spag17* knockout mouse described here demonstrates the most severe phenotype of any reported knockout of a CP gene. Mutations of *Hydin* impair ciliary motility and brain fluid transport, resulting in hydrocephalus (13). Mice lacking Pcdp1 demonstrate an accumulation of mucus in the sinus cavity, hydrocephalus, and sperm with a loss of mature flagella (14). These mutant mice survive the neonatal period, as do the *Spag6* and *Spag16* mutants already noted. Intriguingly, the phenotypes of deletion in each of these proteins are quite different. One possible explanation for the diversity in phenotypes states that

the proximity of the encoded proteins to the radial spokes, which connect to the outer doublets and their dynein motors, determines phenotypic severity. This hierarchy of phenotypic severity underscores the differences between mammalian and nonmammalian axoneme function.

Author disclosures are available with the text of this article at www.atsjournals.org.

Acknowledgments: The authors thank Dr. Elizabeth F. Smith (Department of Biological Sciences, Dartmouth University) for her comments and suggestions, Dr. Jorge Almenara (Anatomic Pathology Research Services, Virginia Commonwealth University) for assistance with the histologic studies, Dr. Lee Lance (Sanford School of Medicine, University of South Dakota) for kindly providing the Pcdp1 antibody, and Dr. Eileen O'Toole (University of Colorado) for assistance with two-dimensional image-averaging analysis.

References

1. Ishikawa H, Marshall W. Ciliogenesis: building the cell's antenna. *Nat Rev Mol Cell Biol* 2011;12:222–234.
2. Lee L. Mechanisms of mammalian ciliary motility: insights from primary ciliary dyskinesia genetics. *Gene* 2011;473:57–66.
3. Goodenough U, Heuser J. Substructure of inner dynein arms, radial spokes, and the central pair/projection complex of cilia and flagella. *J Cell Biol* 1985;100:2008–2018.
4. Smith E, Lefebvre P. The role of central apparatus components in flagellar motility and microtubule assembly. *Cell Motil Cytoskeleton* 1997;38:1–8.
5. Dutcher S, Huang B, Luck D. Genetic dissection of the central pair microtubules of the flagella of *Chlamydomonas reinhardtii*. *J Cell Biol* 1984;98:229–236.
6. Dutcher S. Flagellar assembly in two hundred and fifty easy-to-follow steps. *Trends Genet* 1995;11:398–404.
7. Inaba K. Sperm flagella: comparative and phylogenetic perspectives of protein components. *Mol Hum Reprod* 2011;17:524–538.
8. Zhang Z, Jones BH, Tang W, Moss SB, Wei Z, Ho C, Pollack M, Horowitz E, Bennett J, Baker ME, *et al.* Dissecting the axoneme interactome: the mammalian orthologue of *Chlamydomonas* PF6 interacts with sperm-associated antigen 6, the mammalian orthologue of *Chlamydomonas* PF16. *Mol Cell Proteomics* 2005;4:914–923.
9. Rupp G, O'Toole E, Porter ME. The *Chlamydomonas* PF6 locus encodes a large alanine/proline-rich polypeptide that is required for assembly of a central pair projection and regulates flagellar motility. *Mol Biol Cell* 2001;12:739–751.
10. Wargo MJ, Dymek EE, Smith EF. Calmodulin and PF6 are components of a complex that localizes to the C1 microtubule of the flagellar central apparatus. *J Cell Sci* 2005;118:4655–4665.
11. Zhang Z, Zariwala MA, Mahadevan MM, Caballero-Campo P, Shen X, Escudier E, Duriez B, Bridoux A-M, Leigh M, Gerton GL, *et al.* A heterozygous mutation disrupting the *Spag16* gene results in biochemical instability of central apparatus components of the human sperm axoneme. *Biol Reprod* 2007;77:864–871.
12. Sapiro R, Kostetskii I, Olds-Clarke P, Gerton GL, Radice GL, Strauss JF III. Male infertility, impaired sperm motility, and hydrocephalus in mice deficient in sperm-associated antigen 6. *Mol Cell Biol* 2002;22:6298–6305.
13. Lechtreck K-F, Delmotte P, Robinson ML, Sanderson MJ, Witman GB. Mutations in *Hydin* impair ciliary motility in mice. *J Cell Biol* 2008;180:633–643.
14. Lee L, Campagna DR, Pinkus JL, Mulhern H, Wyatt TA, Sisson JH, Pavlik JA, Pinkus GS, Fleming MD. Primary ciliary dyskinesia in mice lacking the novel ciliary protein Pcdp1. *Mol Cell Biol* 2008;28:949–957.
15. Leigh M, Pittman J, Carson J, Ferkol T, Dell S, Davis S, Knowles M, Zariwala M. Clinical and genetic aspects of primary ciliary dyskinesia/Kartagener syndrome. *Genet Med* 2009;11:473–487.
16. Berg J, Evans J, Leigh M, Omran H, Bizon C, Mane K, Knowles M, Weck K, Zariwala M. Next generation massively parallel sequencing of targeted exomes to identify genetic mutations in primary ciliary dyskinesia: implications for application to clinical testing. *Genet Med* 2011;13:218–229.
17. Zhang Z, Kostetskii I, Tang W, Haig-Ladewig L, Sapiro R, Wei Z, Patel AM, Bennett J, Gerton GL, Moss SB, *et al.* Deficiency of SPAG16L causes male infertility associated with impaired sperm motility. *Biol Reprod* 2006;74:751–759.
18. Pazour G, Witman G. The vertebrate primary cilium is a sensory organelle. *Curr Opin Cell Biol* 2003;15:105–110.
19. Olbrich H, Schmidts M, Werner C, Onoufriadis A, Loges N, Raidt J, Banki N, Shoemark A, Burgoyne T, Al Turki S, *et al.* Recessive *Hydin* mutations cause primary ciliary dyskinesia without randomization of left–right body asymmetry. *Am J Hum Genet* 2012;91:672–684.
20. Brody SL, Yan XH, Wuerffel MK, Song S-K, Shapiro SD. Ciliogenesis and left–right axis defects in Forkhead factor HFH-4–null mice. *Am J Respir Cell Mol Biol* 2000;23:45–51.
21. Ibanez-Tallon I, Gorokhova S, Heintz N. Loss of function of axonemal dynein *Mdnah5* causes primary ciliary dyskinesia and hydrocephalus. *Hum Mol Genet* 2002;11:715–721.
22. Lucas JS, Adam EC, Goggin PM, Jackson CL, Powles-Glover N, Patel SH, Humphreys J, Fray MD, Falconnet E, Blouin J-L, *et al.* Static respiratory cilia associated with mutations in *Dnahc11*/*Dnah11*: a mouse model of PCD. *Hum Mutat* 2012;33:495–503.
23. Araneda O, Tuesta M. Lung oxidative damage by hypoxia. *Oxid Med Cell Longev* 2012;2012:1–18.
24. Turgeon B, Meloche S. Interpreting neonatal lethal phenotypes in mouse mutants: insights into gene function and human diseases. *Physiol Rev* 2009;89:1–26.
25. O'Toole E, Giddings T, Porter M, Ostrowski L. Computer-assisted image analysis of human cilia and *Chlamydomonas* flagella reveals both similarities and differences in axoneme structure. *Cytoskeleton (Hoboken)* 2012;69:577–590.
26. Goduti D, Smith E. Analyses of functional domains within the PF6 protein of the central apparatus reveal a role for PF6 sub-complex members in regulating flagellar beat frequency. *Cytoskeleton (Hoboken)* 2012;69:179–194.
27. Castleman V, Romio L, Chodhari R, Hirst R, de Castro S, Parker K, Ybot-Gonzalez P, Emes R, Wilson S, Wallis C, *et al.* Mutations in radial spoke head protein genes RSPH9 and RSPH4A cause primary ciliary dyskinesia with central-microtubular–pair abnormalities. *Am J Hum Genet* 2009;84:197–209.
28. Zietkiewicz E, Bukowy-Bieryllo Z, Voelkel K, Klimek B, Dmenska H, Pogorzelski A, Sulikowska-Rowins A, Rutkiewicz E, Witt M. Mutations in radial spoke head genes and ultrastructural cilia defects in East-European cohort of primary ciliary dyskinesia patients. *PLoS ONE* 2012;7:e33667.
29. Zhang Z, Kostetskii I, Moss SB, Jones BH, Ho C, Wang H, Kishida T, Gerton GL, Radice GL, Strauss JF III. Haploinsufficiency for the murine orthologue of *Chlamydomonas* PF20 disrupts spermatogenesis. *Proc Natl Acad Sci USA* 2004;101:12946–12951.